Journal Pre-proofs

Unraveling the extracellular matrix-tumor cell interactions to aid better targeted therapies for neuroblastoma

Rebeca Burgos-Panadero, Souhaila H. El Moukhtari, Inmaculada Noguera, Carlos Rodríguez-Nogales, Susana Martín-Vañ ó, Pablo Vicente-Munuera, Adela Cañete, Samuel Navarro, María J Blanco-Prieto, Rosa Noguera

PII: S0378-5173(21)00864-4
DOI: https://doi.org/10.1016/j.ijpharm.2021.121058
Reference: IJP 121058

To appear in: *International Journal of Pharmaceutics*

Received Date: 3 June 2021
Revised Date: 24 August 2021
Accepted Date: 25 August 2021

Please cite this article as: R. Burgos-Panadero, S.H. El Moukhtari, I. Noguera, C. Rodríguez-Nogales, S. Martín-Vañ ó, P. Vicente-Munuera, A. Cañete, S. Navarro, M.J. Blanco-Prieto, R. Noguera, Unraveling the extracellular matrix-tumor cell interactions to aid better targeted therapies for neuroblastoma, *International Journal of Pharmaceutics* (2021), doi: https://doi.org/10.1016/j.ijpharm.2021.121058

Unraveling the extracellular matrix-tumor cell interactions to aid better targeted therapies for neuroblastoma

Rebeca Burgos-Panadero[1,2,†], Souhaila H. El Moukhtari[3,5,†], Inmaculada Noguera[4], Carlos Rodríguez-Nogales[3,5], Susana Martín-Vañó[1,2],Pablo Vicente-Munuera[6], Adela Cañete[7], Samuel Navarro[1,2] María J Blanco-Prieto[3,5*], Rosa Noguera[1,2,*]

[1] Department of Pathology, Medical School, University of Valencia – INCLIVA Biomedical Health Research Institute, 46010 Valencia, Spain; reburpa@alumni.uv.es (R.B-P.), samuel.navarro@uv.es (S.N.), Susana.Martin@uv.es (S.M-V.)

[2] Low Prevalence Tumors, Centro de investigación biomédica en red de cáncer (CIBERONC), Instituto de Salud Carlos III, 28029 Madrid, Spain

[3] Department of Pharmaceutical Technology and Chemistry, School of Pharmacy and Nutrition, University of Navarra, 31008, Pamplona, Spain; selmoukhtar@alumni.unav.es (S.H.E.), crodriguez.31@alumni.unav.es (C.R-N.)

[4] Central Support Service for Experimental Research (SCSIE), University of Valencia, 46100 , Burjassot, Valencia, Spain; Inmaculada.Noguera@uv.es (I.N).

[5] Instituto de Investigación Sanitaria de Navarra (IdiSNA), 31008, Pamplona, Spain

[6] Instituto de Biomedicina de Sevilla (IBiS), Hospital Universitario Virgen del Rocío/CSIC/Universidad de Sevilla and Departamento de Biología Celular, Universidad de Sevilla, Seville 41013, Spain; pvicente1@us.es (P.V-M.)

[7] Pediatric Oncology, La Fe Hospital, Av. Fernando Abril Martorell 106, 46026, Valencia, Spain; canyete_ade@gva.es (A.C.)

* Correspondence: mjblanco@unav.es (MJ.B-P.), Rosa.Noguera@uv.es (R.N.); Tel.: 34-948425679 and 34-963983948

† These authors contributed equally to this work.

Highlights:

- A combination of mathematical and *in vivo* models revealed the role of vitronectin in extracellular matrix-tumor cell interactions in high-risk neuroblastoma patients.
- Vitronectin and its ligands can be potential therapeutic targets in neuroblastoma therapy.
- Nanoencapsulation of etoposide increases its efficacy in neuroblastoma cell lines.
- A synergistic effect is observed in high risk-neuroblastoma cells when cilengitide is combined with etoposide/etoposide nanoparticles.

Abstract: Treatment in children with high-risk neuroblastoma remains largely unsuccessful due to the development of metastases and drug resistance. The biological complexity of these tumors and their microenvironment represent one the many challenges to face. Matrix glycoproteins such as vitronectin act as bridge elements between extracellular matrix and tumor cells and can promote tumor cell spreading. In this study, we established through a clinical cohort and preclinical models that the interaction of vitronectin and its ligands, such as α_v integrins, are related to the stiffness of the extracellular matrix in high-risk neuroblastoma. These marked alterations found in the matrix led us to specifically target tumor cells within these altered matrices by employing nanomedicine and combination therapy. Loading the conventional cytotoxic drug etoposide into nanoparticles significantly increased its efficacy in neuroblastoma cells. We noted high synergy between etoposide and cilengitide, a high-affinity cyclic pentapeptide α_v integrin antagonist. The results of this study highlight the need to characterize cell-extracellular matrix interactions, to improve patient care in high-risk neuroblastoma.

Keywords: tumor microenvironment; nanomedicine; neuroblastoma; cilengitide; etoposide

Abbreviations: CI, combination index; CLG, cilengitide; DRI, dose reduction index; ECM, extracellular matrix; EE, encapsulation efficiency ; ETP, etoposide; Fa, fraction affected; GAGs, glycosaminoglycans; HR-NB, high-risk neuroblastoma; ICC, immunocytochemistry; IHC, immunohistochemistry; INRG, International Neuroblastoma Risk Group; MNA, *MYCN*-amplified; MNNA, *MYCN* non-amplified; NPs, nanoparticles; NB, neuroblastoma; PAI-1, plasminogen activator inhibitor 1; PDI, polydispersity index; SCA, segmental chromosome aberration; TMA, tissue microarray; TME, tumor microenvironment; UHPLC-MS/MS, ultra-high-performance liquid chromatography tandem mass spectrometry; uPAR, urokinase-type plasminogen activator receptor; VN, vitronectin; VN-KO, VN knockout; VN-WT, VN wildtype.

1. Introduction

Tumor growth and metastasis are well known processes in tumor biology, derived from communication signals that tumor cells exchange with their surrounding microenvironment (Ren et al., 2018). Extracellular matrix (ECM) components such as vitronectin (VN) or fibronectin participate in cell-ECM interactions in both tumors and healthy tissues (Xu and Mosher, 2011). VN studies have received increased focus in cancer research during recent years, as this molecule is involved in remodeling tumor microenvironment (TME) and tumor cell heterogeneity through its main ligands such as integrins, urokinase-type plasminogen activator receptor (uPAR) or plasminogen activator inhibitor-1 (PAI-1) (Aaboe et al., 2003; Ortega-Martínez et al., 2016; Zhu et al., 2014). Tumor ECM mechanical properties arbitrate cellular behavior and biological patterns of the disease, triggering aggressive stiff tumor scaffolding (Kalli and Stylianopoulos, 2018). Primary tumor stiffness was found to be greater than in normal tissues and has been linked to cancer progression and metastasis, justifying its use as a potential therapeutic target (Cacho-Díaz et al., 2020; Handorf et al., 2015). Finally, by thoroughly characterizing tumors and their surroundings, higher tumor size reduction could be potentially achieved by combining drugs to specifically target tumors and the tumor-ECM interaction simultaneously.

In that sense, the α_v integrin family is mainly linked to angiogenesis, and experimental data has revealed that $\alpha_v\beta_3$ and $\alpha_v\beta_5$ integrins are highly expressed in tumor blood vessels, thus integrin inhibitors have been proposed as therapeutic agents (Tabatabai, 2017). Tumor cells can also express these integrins (Desgrosellier and Cheresh, 2010) and some inhibitors have been suggested, including cilengitide (CLG or EMD121974), with promising results (Harjunpää et al., 2019). CLG is a small pentapeptide that inhibits both integrins and has been used in preclinical studies in breast cancer, supporting its efficacy against bone metastasis (Bäuerle et al., 2011), and in clinical trials for other malignancies (Gilbert et al., 2012; Haddad et al., 2017; Vansteenkiste et al., 2015). However, CLG is rapidly cleared from the bloodstream and from tumor sites which has impeached this drug to reach the market so far (Stupp et al., 2014b).

Neuroblastoma (NB) is the most frequent solid extracranial malignancy diagnosed in children. High-risk NB (HR-NB) patients have a poor prognosis, with long-term survival rates remaining at only 50% (Matthay et al., 2016). In previous studies, we identified an ultra-HR patient subgroup with 5-year survival rate <15%, defined by tumors with an altered organization of blood vessels and reticulin fibers (Tadeo et al., 2016). Many novel therapies address ECM tumor stiffness, using VN as a target (Burgos-Panadero et al., 2019; DeVita VT, Lawrence TS, 2008; Vicente-Munuera et al., 2020) However, HR-NB studies are limited by a lack of accurate biomarkers of the underlying biological pathways related to ECM stiffness (Burgos-Panadero et al., 2019; Tadeo et al., 2017, 2016, n.d.).

Chemotherapy is the gold-standard treatment for cancer, but its overall toxicity limits the therapeutic benefits in HR-NB (Tsai et al., 2014). A greater understanding of the role of the ECM will bring a crucial insight into the factors potentially shaping the response to a specific treatment cocktail (Cox, 2021). In this regard, the heterogeneous composition of the TME

suggests that targeting its components is useful for combination therapies, as this could reduce side effects and therapeutic resistance (Ribeiro Franco et al., 2020). Nanomedicine and multitargeted therapies have proven to solve these types of quandaries. In fact, nanomedicines have been studied as promising anti-metastatic strategies with the possibility to modulate the TME while improving the therapeutic index of drugs (Chen et al., 2020; Overchuk and Zheng, 2018). We decided to nanoencapsulate etoposide (ETP), a very hydrophobic podophyllotoxin derivative used in combination with other anticancer drugs in HR-NB (Lange et al., 2003). This drug is often associated with acute and late toxicities and could potentially benefit from nanotechnology (Relling et al., 1998). In this sense, the synergism between CLG and nanoencapsulated ETP could be vital in ameliorating therapeutic perspectives for HR-NB patients (Liang et al., 2016; Yang et al., 2020). Finally, by attacking tumors on several fronts, these treatments could afford optimal results by inhibiting complementary molecular targets in HR-NB.

2. Materials and Methods

2.1. Patient cohort

We analyzed 127 primary NB tumors (at least two representative cylinders of 1 mm) included in tissue microarrays (TMAs) received at Incliva Biomedical Research Institute between 2000 and 2015. In this study cohort, a 30% of the patients were classified as HR-NB. Morphometric and topological quantification was focused on 91 samples with single nucleotide polymorphism array results. Samples were classified by genetic instability criteria based on SCAs and gene amplification into very low (profiles without SCAs); low (≤3 typical or recurrent NB SCAs, excluding 11q deletion (11qD)); medium (profiles with 11qD or *MYCN*-amplified (MNA) or >3 typical SCAs); and high (profiles with chromothripsis, or > 3 gene amplifications). The clinical and biological data of the whole cohort are summarized in **Table S1**. The study was approved by Incliva's Clinical Research Ethics Committee (ref. B.0000339).

2.2. Tumor xenografts

All experiments performed in VN−/− (B6.129S2 (D2)-Vtntm1Dgi/J) and RAG1−/− (B6.129S7-Rag1tm1Mom/J) complied with the standards and care approved by the Institutional Animal Care Ethics Committee (reference 2015/VSC/PEA/00083). The *in vivo* experiment described in this research was performed using homozygous mice: RAG1-/- VN-/- (experimental or VN knockout, VN-KO) and RAG1-/- VN+/+ (control or VN wildtype, VN-WT). Orthotopic HR-NB xenografts were generated using 1×10^6 SH-SY5Y and SK-N-BE (2) cells lines in four-to six-week-old mice. Detailed experimental procedure and additional information are described in the Supplementary Materials and Methods.

2.3. Cell Culture

The HR-NB cell lines used (**Table 1**) were purchased from the ATCC (American Type Culture Collection). All cell lines were grown under 5% CO2 at 37°C. The cell lines were maintained in Iscove's Modified Dulbecco's Medium (IMDM), supplemented with 10% (except CHLA-90 with 20%) heat-inactivated fetal bovine serum (FBS), 1% of insulin-transferrin-selenium (ITS), and 100 U/mL penicillin/100 µg/mL streptomycin. All the reagents were acquired from Gibco, Thermo Fisher Scientific Inc., Waltham, MA, USA. Immunocytochemistry (ICC) and genetic data (**Table 1**) guided the choice of the two most representative HR-NB cell lines for orthotopic implantation in mice.

Table 1. Summary of NB cell lines

Analyzed features		**Cell lines**					
		SK-N-BE (2)	**NGP**	SH-SY5Y	CHLA-90	SK-N-SH	NBL-S
VN	% positive cells	70%	80%	70%	50%	50%	30%
	Intensity	+++	70% (++) 10% (+++)	++	30% (++) 20% (+++)	+	+
	Location	Cell membrane and neuritic projections		Cytoplasm		Cell membrane	
uPAR	% positive cells	15%	30%	90%	80%	Negative	
	Intensity	++	++	+++	50% (+++) 30 (++)		
	Location	Cytoplasm	Cytoplasm and Golgi pattern	Golgi pattern	Cytoplasm		
PAI-1	% positive cells	20%	10%	40%	20%	Negative	
	Intensity	+	+	++	+		
	Location	Cytoplasm					
$\alpha_v B_3$	% positive cells	10%	10%	85%	50%	20%	20%
	Intensity	+	+	80% (++) 5% (+++)	++	++	+
	Location	Cytoplasm. In case of CHLA-90, also in cell membrane.					
α_v	% positive cells	60%	40%	70%	40%	20%	40%
	Intensity	++	++	++	++	++	++
	Location	Cytoplasm					
B_5	% positive cells	Negative					

Chromosomal aberrations	1p- ((cnLOH pter- p21.3), (p21.3-p12)), +1q(q11-qter), 3p-(pter-p14.2), +11q(q13.1-qter), +17q (q12-qter), ALK WT, p53 (p.C135F)	1p- (cnLOH pter-p32.3), 3p- (pter-p25.3), 11q- (q22.1-qter), +17q (q21.1-qter), ALK WT, p53 (p.A159D, p.C141W)	+1q (q12-q44), +2p (pter-p16.3), +17q (q21.31-qter), ALK (F1174L), p53 WT	+11q, p53 (p.E286K), ALK (p.F1245V)	+2p (pter-p16.3), +17q (q21.31-qter), ALK (p.F1174L), p53 WT	11q- (q14.1-qter), ALK WT, p53 WT

MYCN-amplified cell lines are highlighted in bold. These NB cell lines were used for the characterization of VN and its ligands. These cell lines guarantee a wide representation of morphological and molecular features in HR-NB *in vitro*. Other suitable NB cell lines that can be used for this type of study can be classified by *MYCN* amplification (MNA (Kelly, LAN1, LAN5, IMR32) and MNNA (IMR32, SK-N-AS, NB-69, LAN6), since this is one of the main signatures found in HR-NB, and is associated with an aggressive tumor phenotype (Harenza et al., 2017). Immunoreactivity of the analyzed markers was scored using a combination of positive cells with a degree of staining intensity and localization pattern. Genetic information obtained from references: (Brodeur et al., 1977; Carpenter et al., 2014; Harenza et al., 2017; Kryh et al., 2011; Stock et al., 2008). HR-NB:high-risk neuroblastoma ; MNA:*MYCN*-amplified; MNNA: *MYCN* non-amplified;VN: vitronectin; uPAR: urokinase-type plasminogen activator receptor; PAI-1: plasminogen activator inhibitor 1; cnLOH: copy neutral loss of heterozygosity; WT:wild-type.

2.4. Identification of microscopic tumor components

TMA paraffin blocks derived from NB patients and xenografts were cut (3 μm) and stained using histochemical and immunohistochemical (IHC) analysis. For ICC analysis, adherent cells were seeded in cell chamber 8-well slide (PLC30108, SPL LifeSciences) and cytocentrifugation was used to deposit non-adherent cells onto poly L-lysine coated slides using Shandon CytoSpin III Cytocentrifuge at 1200 rpm for 10 min. Cells were fixed with methanol/acetone (1:1) for 10 min at room temperature and subsequently immunostained with the selected antibodies. Immunoreactivity was independently assessed and approved by two researchers. We performed a microscope assessment of the biomarkers following these staining criteria: 1) a score based on the proportion of positive cells over total cells (percent positivity) ranging from 0 to 100%; 2) staining intensity was evaluated as 0 = negative, 1+ = weak, 2+ = moderate, and 3+ = strong, and 3) localization pattern in order to determine protein expression. This semi-quantified analysis was used to set image analysis parameters. All immunostained slides were digitized with the whole-slide Pannoramic MIDI scanner (3DHISTECH Ltd., Budapest, Hungary) at 20x magnification. For morphometric analysis, we developed customized macros using Image Pro-plus (Media Cybernetics), adjusted individual modules (DensitoQUANT, NuclearQUANT, MembraneQUANT, Pannoramic viewer (3DHISTECH)) and customized configurations using the designed-tool Angiopath. Topological analysis was only applied to VN using Matlab R2014b (MathWorks). Conditions, antibodies and a description of the image analysis approach and parameters obtained is summarized in supplementary **Table S2.**

2.5 Formulation and characterization of etoposide nanoparticles (ETP-NPs)

ETP-loaded nanoparticles (ETP-NPs) were prepared by hot homogenization and ultrasonication method and then freeze-dried for further studies as previously described, but with slight modifications (Estella-Hermoso de Mendoza et al., 2008) Briefly, the lipid phase consisted of 300 mg of Precirol ATO 5 with 5 mg ETP, while the aqueous phase consisted of 10 mL of a 2% (w/v) Tween® 80 aqueous solution. The nanoparticle suspension obtained was subsequently cooled in an ice bath for 15 minutes and washed three times with filtered water by diafiltration at 50000 g for 30 minutes to remove excess surfactant and non-incorporated drug. ETP-NPs were then resuspended in an aqueous solution of trehalose and freeze-dried. The size and the polydispersity index (PDI) of the nanoparticles (NPs) were determined in triplicate by photon correlation spectroscopy and zeta potential by laser Doppler anemometry, using a Zetasizer Nano (Malvern, UK). Each experiment was performed in triplicate. All data are expressed as a mean value ± standard deviation. The amount of ETP entrapped into the NPs was calculated using ultra-high performance liquid chromatography–tandem mass spectrometry UHPLC-MS/MS method after extracting the drug from the NPs using a mixture of chloroform and methanol (1:1). After centrifugation, ETP was quantified and results and data were analyzed using the Mass Lynx^{TM} NT 4.1 Software with QuanLynx^{TM} program (Waters Corp, Milford, MA, USA.

2.6. Cytotoxicity and drug combination studies

The antitumor activity of ETP, ETP-NP and CLG was studied with MTS assay in HR-NB cell lines. First, 5000 cells per well were seeded in tissue culture 96 well-plates for all HR-NB cell lines except for NGP cell line (20000 cells per well). The day after, these cells were exposed to increasing concentrations of ETP, CLG and ETP-NP for 72h. The half maximal inhibitory concentration (IC50) was then obtained with GraphPad Prism 9 software (GraphPad La Jolla, California, USA). Results are expressed as the mean data ± standard deviation (SD) of at least three independent determinations. Data obtained from MTS assays and processed with GraphPad Prism 9 (IC_{50}) were statistically analyzed using a one-way ANOVA analysis paired t test with Turkey post hoc correction, considering a 95 % confidence interval at a significance level $p<0.05$.

For drug interaction analysis free and nanoencapsulated ETP were combined with CLG at different ratios using cell viability assays as described above by MTS assay. The effect of combination treatments was evaluated by the determination of the combination index (CI) according to the Chou-Talalay method (Chou, 2010). The CI values are defined as follows: CI < 1 indicates synergism; CI = 1 additivity, and CI > 1 antagonism. Dose reduction index (DRI) of ETP, ETP-NP and CLG was calculated and defined as the measure of the dose fold decrease for each drug when synergistically combined to achieve a given effect, compared with the dose of each drug alone required to engender the same inhibition. Detailed information regarding the chemicals is described in the Supplementary Materials and Methods.

2.7. Statistical analysis

Statistical analyses were conducted using SPSS 26.0 software (SPSS Inc., Chicago, IL, USA). The association between cell expression, ECM elements stained and clinical-biological features was analyzed using χ^2 test. Survival analysis was carried out using Kaplan-Meier curves and log-Rank test. To select TME candidates, we first performed univariate and discriminant analysis (Fisher's discriminant function coefficients). Stepwise forward logistic regression was performed to assess the contribution of morphometric, clinical, and genetic features to the proposed pre-treatment risk classification and genomic instability subtypes. We considered p-values less than 0.05 as statistically significant.

3. Results

3.1. Morphometric and topological patterns of territorial VN and blood microvascular structures as clinically relevant biomarkers in human tumors

In the 91 NB patient cohort (**Table S1**) a selection of previous and new statistically significant morphometric and topological features of ECM elements and vessels were extracted and added to the International Neuroblastoma Risk Group (INRG) unfavorable independent variables to classify patients according to pre-treatment risk stratification and tumor genetic instability criteria (**Figure S1**). After logistic regression, variables that predicted the pre-treatment risk groups were placed in the following order of importance: age, sinusoidal shape, stage, Euler number (indicating the compactness of territorial VN), and *MYCN* status (**Table 2**). This model improved specificity (0.94 vs. 0.89) with a slight decrease in sensitivity (0.70 vs. 0.75) compared to the model we previously described (Vicente-Munuera et al., 2020). The variables that best predicted groups of high and low tumor genetic instability were: *MYCN* status, age, number of branches per node (number of crosslinks) of territorial VN, presence of segmental chromosome aberrations (SCAs), and deformity of post-capillaries/metarterioles (**Table 2**). This model also improved specificity (0.96 vs. 0.91), with equal sensitivity (0.89) to the previously used model (Vicente-Munuera et al., 2020). Kruskal-Wallis analysis noted that tumors with high expression of territorial VN presented greater area and length of blood vessel capillaries (p= 0.001 and 0.002, respectively), less sinusoidal deformity (p=0.03) and larger perimeter of total blood vessels (p=0.022).

Table 2. Multivariate logistic regression.

Features	B	SE	Z-score	Pr(>|z|)
Pre-treatment risk stratification group				
(Intercept)	-1.63	1.16	-1.40	0.16
Blood vessels_2050_Shape	-0.83	0.30	-2.81	0.004
Age (≥ 18 months)	2.69	0.66	4.08	4.48e-05
Stage (M)	-0.006	0.01	-0.51	0.61
MYCN (MNA)	-0.004	0.01	-0.35	0.73
Euler number of territorial VN	0.49	0.28	1.73	0.08
Tumor genetic instability criteria				
(Intercept)	-25	4902.30	-0.005	0.99

Blood vessels_1520_Deformity	-0.78	0.48	-1.61	0.11
Age (≥ 18 months)	3.08	1.23	2.50	0.01
Genetic profile (SCA)	20.31	4902	0.004	0.99
MYCN (MNA)	23.44	4912.94	0.005	0.99
Branches per node of territorial VN	1.93	0.70	2.76	0.005

Models using the final set of features for each criterion. Each model is defined by the different coefficients (B column) of the intercept and independent variables (features). SE stands for standard error. Z-score and its associated p-value are represented. M: metastatic; SCA: segmental chromosomal aberration; MNA: *MYCN*-amplified; VN: vitronectin. Blood vessels_2050 (sinusoids vessels). Blood vessels_1520 (post-capillaries/metarterioles vessels).

3.2. Translation from hallmarks of microenvironmental components in xenografts to matrix-centric therapies

The characteristics associated with stiffness of the ECM described in aggressive NB patients [23,25-28,37] are maintained in the tumor passages of orthotopic models. SK-N-BE (2) derived xenografts show a decrease in glycosaminoglycans (GAGs) along with an increase in reticular fibers. In contrast, the amount of collagen type I decreased in advance passages in the VN-KO model, whereas non-remarkable differences were observed in SH-SY5Y-derived xenografts. The orthotopic models are vascularized tumors characterized by tortuous vessels (blood and lymphatic), and differences were noted at the lymphatic level. SK-N-BE (2)-derived xenografts were characterized by a decrease in the amount of lymph vessels in VN-KO mice; in SH-SY5Y-derived xenografts, the quantity of lymph vessels also decreased in advanced passages in both mice backgrounds. In the immune cell infiltration compartment, we observed clusters in stroma and single cells in perivascular areas, with no major difference between xenografts (**Figure 1** and **Figure S2**).

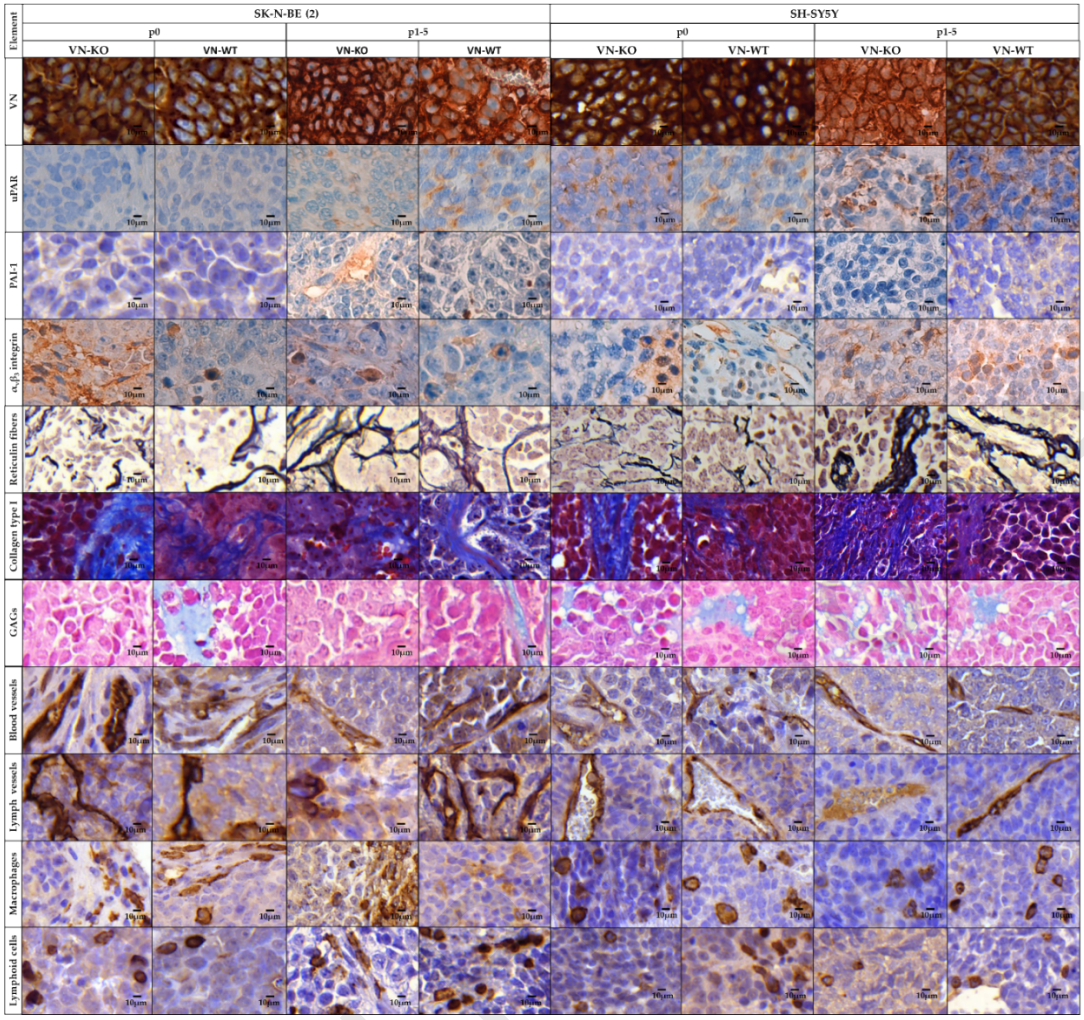

Figure 1. Histological sections of different stains of tumor microenvironment elements in *MYCN*-amplified (SK-N-BE (2) and non-amplified (SH-SY5Y) derived xenografts. Images at 63x. WT: wild-type; KO: Knockout; VN: vitronectin; uPAR: urokinase-type plasminogen activator receptor; PAI-1: plasminogen activator inhibitor 1; GAGs: glycosaminoglycans; p: passage.

3.3. Known VN ligands are significant in HR-NB biology

In the 127 NB patient cohort (**Table S1**), the number of available cases for VN ligands was lower due to a lack of representative tissue for this analysis. uPAR expression was limited to immune stromal cells in 27% of samples (20/75), of which 18 samples also had positive endothelial cells (**Figure 2A**). In addition, we also found two samples with nonspecific immunoreactivity in ganglion cells, which were excluded from statistical analysis. With PAI-1 staining, we observed that 27% of samples (21/78) were positive: 11 cases in tumor cells (nuclear and prolongation staining) and 10 cases in endothelial and blood cells (leukocytes and erythrocytes) (**Figure 2B**). Using the Chi-square test, we found a statistical association between PAI-1 expression in MNA tumor cells (p= 0.037) and HR patients (p= 0.015). With respect to survival, using the log-rank test we found a significant statistical relationship between PAI-1 expression in tumor cells and higher relapse rates (5-year EFS% 30±14.5) (**Figure S4**). Concerning $\alpha_v\beta_3$ integrin expression, we found that 43% of the samples (32/75) were positive in endothelial cells and monocyte/macrophage lineage cells (**Figure 2C**). Again, with Chi-

square test, we found a statistical association between $\alpha_v\beta_3$ integrin expression in endothelial cells and 17q gain in tumor cells (p= 0.028).

In vitro, noticeable differences were observed in the percentage of positive cell and intensity staining of uPAR, PAI-1 and $\alpha_v\beta_3$ integrin (low in MNA and moderate–high in half of *MYCN* non-amplified (MNNA) cell lines), and negative expression of β_5 integrin was present (**Table 1** and **Figure S3**).

In vivo, neuroblastic cells significantly increased VN expression compared to *in vitro* conditions, without observed differences between the two mice models of cell lines. Notably, uPAR expression was altered from negative to positive in SK-N-BE (2)-derived p1-5 xenografts (p=0.048 in VN-KO and 0.034 in VN-WT) contrasting with continuous positive expression in SHSY5Y-derived xenografts passages. No important distinction was found between passages of the two cell lines as regards PAI-1 expression. An increase in $\alpha_v\beta_3$ integrin expression was however observed, especially in SK-N-BE (2)-derived p0 xenografts with the VN-KO background (p=0.017) (**Figure 1** and **Figure S2**).

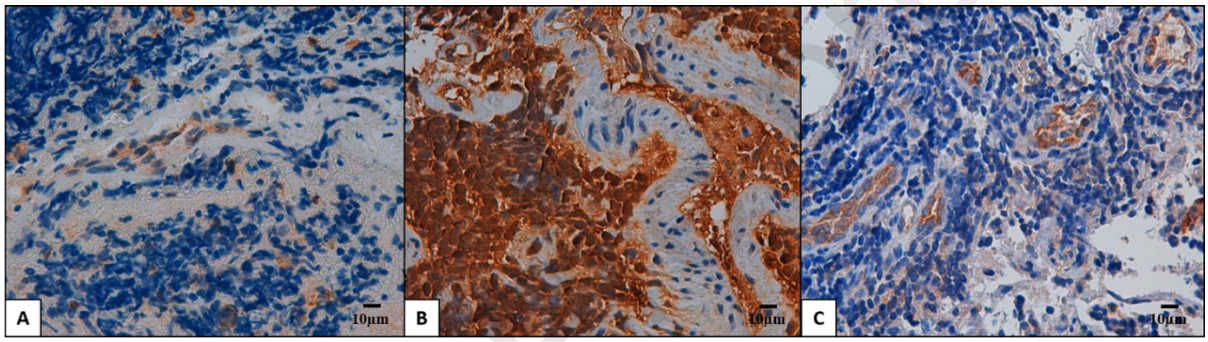

Figure 2. VN ligand expression patterns in neuroblastic tumors: a) uPAR positivity in endothelial and stromal immune cells; b) PAI-1 expression in tumor cells, nuclear and neuropile; c) α_vB_3 integrin expression in endothelial cells. Immunostained images at 40x. VN: vitronectin; uPAR: urokinase-type plasminogen activator receptor; PAI-1: plasminogen activator inhibitor 1.

3.4. Physicochemical characterization of ETP nanomedicine

ETP-NP exhibited a mean hydrodynamic diameter close to 100 nm (*i.e.,* 107.53 ± 2.15 nm) and a homogenous distribution with a PDI of 0.193 ± 0.03. The surface charge of the proposed nanomedicine reflected that those particles were negatively stabilized (-21.93 ± 3.35 mV). ETP-NP showed a high encapsulation efficiency (EE) of around 75% corresponding to a drug loading value of 5.03 ± 0.76 µg/mg.

3.5. Cytotoxicity studies in HR-NB cell lines

All treatments were tested at 72h in 6 different HR-NB cell lines. For CLG, results showed a direct anticancer activity (**Figure 3A**) although this activity is independent from the $\alpha_v\beta_3$ and $\alpha_v\beta_5$ integrin expression previously determined in **Table 1**. CLG cytotoxicity assay in **Figure 3A** shows that this α_v inhibitor has no effect on SH-SY5Y and SK-N-SH cells, despite their high-intensity $\alpha_v\beta_3$ integrin expression even at different cell percentages. In this regard, CLG had a moderate dose-dependent effect on NGP and CHLA-90 cells while having a stronger

dose-dependent effect on SK-N-BE (2) and NBL-S cell lines, independent of intensity and percentage of $\alpha_v\beta_3$ integrin expression (**Figure 3B**). IC_{50} values were established for SK-N-BE (2) (IC_{50}=2.66 ± 1.20 µM) and NBL-S cells (IC_{50}= 0.33 ± 0.2 µM) and these cell lines were chosen to study the synergetic effect with ETP and ETP-NP.

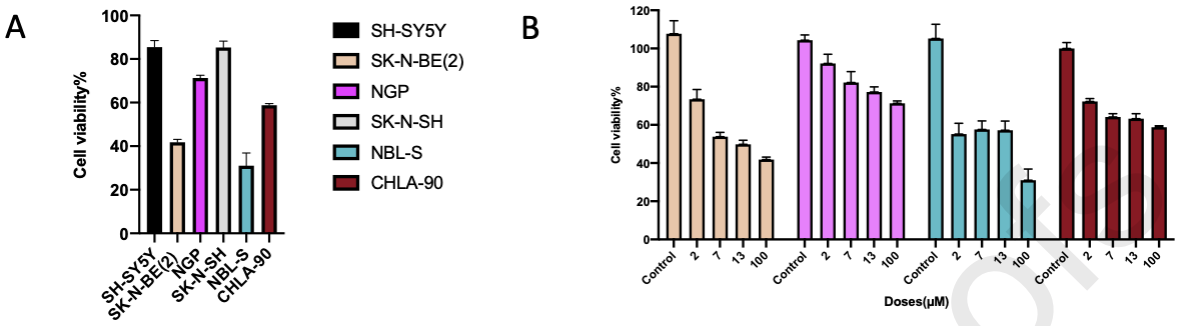

Figure 3. Cell viability assay after cilengitide (CLG) administration. (A) Cell viability at 72h in HR-NB cell lines after a single administration of 100 µM CLG aqueous solution. Values are the mean ± standard deviation (SD) of at least three independent determinations. (B) Cell viability at 72h after 2, 7, 13, 100 µM of CLG aqueous solution in CLG-sensitive cell lines: SK-N-BE (2), NGP, NBL-S and CHLA-90. Values are the mean ± standard deviation (SD) of at least three independent determinations.

Cytotoxicity assays revealed similar or increased efficacy for ETP and ETP-NP in HR-NB cell lines, suggesting that the encapsulation process did not affect ETP antitumor efficacy (**Figure 4A and 4B**). Nanoencapsulation enhanced the anticancer activity of ETP in SK-N-BE (2), CHLA-90 and SH-SY5Y cell lines, by reducing the IC_{50} value as mentioned in **Figure 4C.** Interestingly, in CHLA-90 the IC_{50} was reduced by around 56% with nanoencapsulation from 18 µM with ETP to 8 µM when employing ETP-NP, which provide statistically significant and illustrating the greatest amelioration in chemotherapy sensitivity (**Figure 4C**).

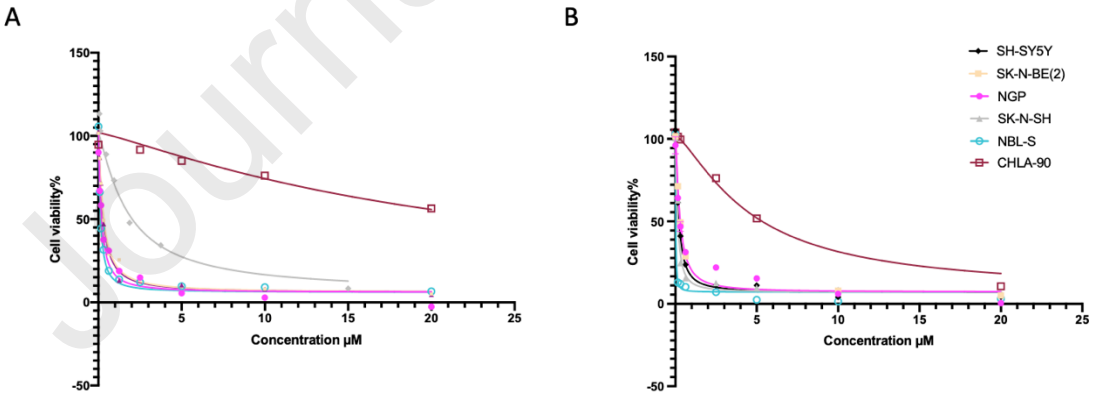

C

	SH-SY5Y	SK-N-BE (2)	NGP	SK-N-SH	NBL-S	CHLA-90
ETP	1.2 ± 0.3	0.8 ± 0.1	0.2 ± 0.1	0.19 ± 0.05	0.05 ± 0.01	18 ± 4
ETP NP	0.25 ± 0.04	0.3 ± 0.1	0.31 ± 0.01	0.16 ± 0.04	0.04 ± 0.03	8 ± 2

Figure 4. Cell viability assays. (A) Cells were exposed to increasing concentrations of etoposide (ETP); (B) Cells were exposed to increasing concentrations of etoposide-loaded nanoparticles (ETP-NP); (C) IC_{50} values (μM) of ETP and ETP-NP in HR-NB cell lines after 72h of treatment. Values are the mean ± standard deviation (SD) of at least three independent determinations.

3.6. CLG combined with ETP or ETP-NP act synergistically against HR-NB cell lines

To study whether the antitumor effect of CLG in HR-NB cells was synergetic with ETP and ETP-NP, SK-N-BE (2) (MNA) and NBL-S (MNNA) cell lines were exposed to individual or combined treatments. When combining CLG and ETP, the DRI of ETP was around 1.89 to 2.92-fold in either its free or nanoencapsulated form in both cell lines at fraction affected (Fa)=0.5.

First, it was necessary to determine the optimal drug ratio in both cell lines, among which ratios 1:2 and 1:1 (CLG:ETP) were considered to achieve optimal CI and DRI. The combined treatment proved synergistic in both cell lines at the proposed ratios (CI<1) (**Figure 5**). **Figures 5A** and **5B** show that the synergistic effect is maintained at all Fa cell death using the 1:1 ratio in both cell lines, thus the 1:1 ratio was selected as optimal to combine these drugs. Finally, the CI value appears to be similar when ETP is administered within nanomedicine at the selected ratio (1:1), indicating that the synergy between the two drugs is maintained when ETP is nanoencapsulated.

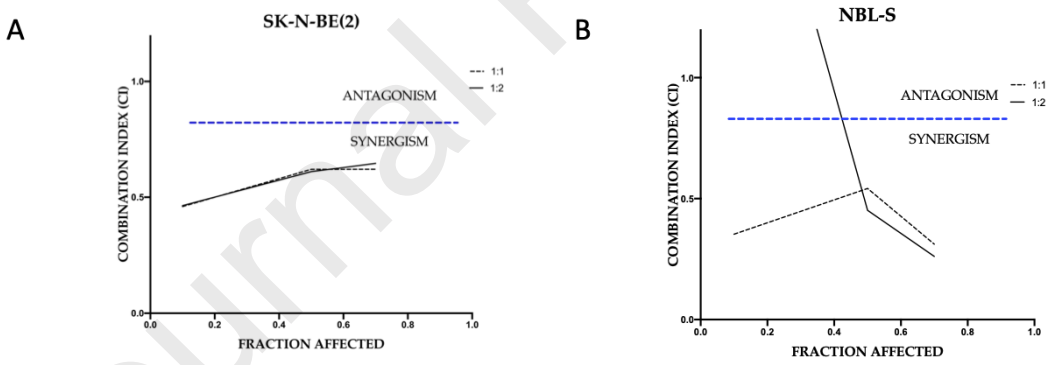

Figure 5. Combination index (CI) analysis graphical representation for etoposide (ETP) and cilengitide (CLG) [cilengitide: etoposide] in SK-N-BE (2) (A) and NBL-S(B) cell lines at different cell viability fractions. CI < 1, synergism; CI=1, additivity; CI>1 antagonism.
nanoencapsulated.

Table 3. Synergy study for cilengitide (CLG) and etoposide (ETP) combination therapy at the IC_{50} in NBL-S and SK-N-BE (2) cell lines after 72 hours of treatment. Drug ratio is expressed as follows: CLG [μM]: ETP [μM]. Values are the mean ± standard deviation (SD) of at least three independent determinations.

	Treatment	Ratio (CLG: ETP)	DRI ETP	DRI CLG	CI
SK-N-BE (2)	ETP	1:1	2.5 ± 0.6	5.60± 2.6	0.6 ± 0.1
		1:2	1.9 ± 0.7	27 ± 12	0.6 ± 0.1
	ETP-NP	1:1	1.8 ± 0.4	5.7 ± 2.7	0.7 ± 0.1
NBL-S	ETP	1:1	2.9 ± 1.5	14 ± 6	0.5 ± 0.3
		1:2	2.7 ± 0.2	13 ± 4	0.5 ± 0.03
	ETP-NP	1:1	2.4 ± 0.7	6. ± 0.8	0.6 ± 0.2

4. Discussion

The stromal architecture of tumors can present a chaotic pattern that stimulates tumor cell spread. Our aim was to investigate the contribution of ECM stiffness to NB, and determine whether targeting ECM-cell interactions could be applied in combination with classic chemotherapy (Fares et al., 2020). In this study, ECM and tumor cells were considered simultaneously, reprograming the TME by inhibiting the VN-integrin interaction with the resulting DNA strand breaks (López-Carrasco et al., 2020). In addition, we explored whether the nanoencapsulation of a chemotherapeutic can potentially ameliorate the therapeutic index of this drug, as we previously demonstrated for osteosarcoma (González-Fernández et al., 2018, 2017).

Several groups have identified key roles for the ECM in facilitating migration transformations, proposing that rigidity of tumor stroma can be attributed to abnormal deposition and remodeling of ECM elements (Craig et al., 2020; Lu et al., 2012). In the present study we highlight the clinical importance of TME microscopy structures in HR-NB, using high-throughput approaches (*i.e.,* computer tools). These tactics are reliable methods to discover potential biomarkers or targets related to stiffness that implies an acceleration in diagnosis, prognostic prediction, and therapy response (Lee et al., 2019; Zormpas-Petridis et al., 2021) In fact, developing and refining high-throughput technologies enable to determine the composition and map the spatial complexity of the three-dimensional tumor matrix and cell plasticity (Cox, 2021). These advances have allowed us to re-examine archived tissues for in-depth study of the role of the matrix in HR-NB.

Digital pathology allowed us to better identify the components of the TME elements analyzed associated with aggressiveness in MNA HR-NB. Our previously published findings in NB samples from patients with poor prognosis (Burgos-Panadero et al., 2019), together with the present studies, indicate that VN synthesis by malignant cells could converge with the formation of stiff pathways. This stiffness facilitates cell leakage and invasion by allowing easy attachment-detachment cycles between cells and collagen III fibers and/or GAGs. The role of VN in this interaction has also been demonstrated by several studies in different malignancies (Schneider et al., 2016; Shi et al., 2015). The gradual stiffening of tumor stroma is confirmed by the orthotopic HR-NB xenograft model studied: ECM element modifications imply that this

model recreates matrix features observed in HR-NB patients with poor prognosis. Interestingly, high expression of integrin $\alpha_v\beta_3$ was found in this orthotopic HR-NB xenograft model, with substantially increased expression in the initial passages of the VN-KO tumor model. However, there is a lack of correlation between integrin $\alpha_v\beta_3$ expression in HR-NB and *in vitro* cell lines and aggressiveness or MNA, respectively. This can be explained by the need to create anchorage points for tumor proliferation, while maintaining stable positive expression in successive passages to promote migration. These results evidence the interaction between VN and $\alpha_v\beta_3$ integrin in HR-NB, as reported in ovarian cancer, where it has been shown that tumor cells achieve rapid migration by MMP-2 cleavage of VN-$\alpha_v\beta_3$ integrin and fibronectin-$\alpha_5\beta_1$ integrin interactions (Kenny et al., 2008). Some studies showed increased expression of VN receptors to be related to poor prognosis in NB patients (Erdreich-Epstein et al., 2016; Li et al., 2004; Sugiura et al., 1999). Interestingly, the interplay between other molecules whose genetic changes were detected in SK-N-BE (2)/MNA cell line in VN-KO model and stiff 3D bioprinted model (López-Carrasco et al., 2020) has also been reported to possibly affect cell adhesion- and migration-related intracellular pathways (Chandrasekar et al., 2003; Moreno-Layseca and Streuli, 2014). Xenografts derived from the SK-N-BE (2)/MNA cell line in the VN-KO model are characterized by increased VN secretion, dynamic expression of $\alpha_v\beta_3$ integrin and high uPAR expression added to the genetic changes described (López-Carrasco et al., 2020), which can be considered as key biomimetic markers in aggressive HR-NB preclinical models. Taking our data into account, high VN expression in MNA and 17q gain tumors with PAI expression in some of its tumor and stroma cells, $\alpha_v\beta_3$ integrin expression in malignant neuroblasts and endothelial cells, imply that these molecules could develop a multifunctional role, which reinforces the predominant role of tumor stroma in tumorigenesis, prognosis, and the search for specific therapeutic targets.

In a second step, after demonstrating the clinical relevance of the VN-integrin interaction and ECM stiffness in HR-NB poor prognosis, we decided to target this union by using a $\alpha_v\beta$ inhibitor. In addition, the combination of morphometric and topological analysis highlighted an increase of VN and larger blood vessels that defined NB with high instability and indicated that they belonged to a high pre-treatment risk group. This size alteration of blood vessels could be related to angiogenesis processes, considering that we implemented the use of anti-angiogenic therapy as CLG to impair the tumor vasculature and VN-integrin interactions. In that sense, CLG efficacy is thought to be due to the reduction of proliferation by inducing cell detachment and apoptosis through binding to and inhibiting $\alpha_v\beta_3$ and $\alpha_v\beta_5$ integrins (Mas-Moruno et al., 2010)**.** Our results show that CLG is effective in HR-NB VN-secreted cells and that sensitivity to CLG is independent from $\alpha_v\beta_3$ integrin expression in pre-treatment HR-NB cells. This data could reflect a transition from low to high affinity state induced by intracellular signaling events or by CLG high-affinity $\alpha_v\beta_3$ ligand in certain HR-NB cell lines. A potential explanation is the proposal of Cheng *et al.,* (Cheng et al., 2014) in a study of malignant pleural mesothelioma, where they establish a relationship between anoikis (cell detachment-mediated death) and CLG sensitivity. Although previous studies in NB and glioblastoma have found a positive correlation between growth inhibition by CLG and $\alpha_v\beta_3$ expression (Leblond et al., 2013). The potential role of $\alpha_v\beta_5$ (the second integrin targeted by CLG) in these effects is unlikely to be significant since it is not expressed at the tumor cells (Erdreich-Epstein et al., 2000). Additional

interactions between tumor cells and VN, as well as signaling events and cell plasticity, could provide CLG resistance.

In a recent study in HR-patients, extended induction chemotherapy added to standard chemotherapy failed to improve patient outcome and increased the number of side-effects (Berthold et al., 2020). Differences in chemotherapy sensitivity can be explained, among other reasons, by NB cell plasticity capable of switching between adrenergic and mesenchymal phenotype (van Wezel et al., 2019). Nano-based therapy holds several advantages over conventional chemotherapy, as it ameliorates the therapeutic drug index and preferentially distributes anticancer agents towards tumor sites (Zhao et al., 2018). In this sense, we previously documented an increase of the efficacy of chemotherapeutic drugs when included into NPs (Garbayo et al., 2020). Lipid NPs are known to efficiently encapsulate hydrophobic molecules, like ETP, and they make possible to conceive oral administration in cancer treatment (el Moukhtari et al., 2021). Furthermore, the lipid used in the formulation of lipid NPs are biodegradable and physiological lipid with GRAS status (generally recognized as safe by the FDA) (Keck and Müller, 2013; Lasa-Saracibar et al., 2012). Additionally, these NPs are easy-to-produce at large scale, which is a major advantage for clinical translation (Joshi and Müller, 2009; Lasa-Saracíbar et al., 2014; "Let's talk about lipid nanoparticles," 2021). We noted that nanoencapsulated ETP improved or maintained *in vitro* efficacy compared to free ETP in all the studied cell lines, indicating an improvement of the therapeutic efficacy of the drug. As an example, drug resistance of CHLA-90 to ETP has been reported in the literature and the IC_{50} was reduced by 56% in our study due to nanoencapsulation (Keshelava et al., 1998).

Finally, strong synergy was noted when co-administrating CLG with ETP in both free and nanoencapsulated form in SK-N-BE (2) and NBL-S cell lines. This data suggested that their combination is likely to enhance overall effectiveness of HR-NB treatment by targeting both the TME and the nucleus of tumoral cells (Hu and Zhang, 2012). The results also indicate that combination therapy using CLG could be useful to reduce the conventional chemotherapy required. In a phase III clinical trial (the CENTRIC EORTC 26071-22072 study), it was reported that CLG did not improve overall survival in glioblastoma patients when combined with temozolomide (Stupp et al., 2014a). This lack of efficacy was attributed to the rapid elimination from the tumor site and short half-life of the drug, a drawback which could easily be overcome by nanoencapsulation or co-vectorization with ETP-NP. It is noteworthy that a low CI value or strong synergism is similar for both CLG:ETP and CLG:ETP-NP combinations, suggesting that synergy is maintained when employing nanovectors instead of free drug delivery. This synergism enables reduced chemotherapy toxicity and establishes CLG as a potential candidate to treat HR-NB in a combined treatment setting. Although these findings will have to be confirmed *in vivo* in animal models of NB, the data presented in this study highlight the importance of characterizing the cell-ECM interactions in HR-NB for the development of targeted therapies.

Acknowledgments

The authors are grateful to the Spanish Society of Pediatric Hemato-Oncology (SEHOP) for patient data management. The authors also thank Kathryn Davies for English corrections and Luis M. Escudero for digital analysis.

Funding

This work was supported by grants from ISCIII and ERDF [PI17/01558] and [PI20/01107]; CIBERONC [contract CB16/12/00484]; Asociación Española contra el Cáncer [FAECC2015/006]; NEN Association [Nico contra el cancer infantil 2017 – PVR00157] and the Neuroblastoma Foundation [PVR00166].

Conflicts of Interest

The authors declare no conflict of interest. The funders had no role in the design of the study; in the collection, analyses, or interpretation of data; in the writing of the manuscript, or in the decision to publish the results.

References

Aaboe, M., Offersen, B. V, Christensen, A., Andreasen, P.A., 2003. Vitronectin in human breast carcinomas. Biochimica et Biophysica Acta (BBA) - Molecular Basis of Disease 1638, 72–82. https://doi.org/https://doi.org/10.1016/S0925-4439(03)00059-0

Bäuerle, T., Komljenovic, D., Merz, M., Berger, M.R., Goodman, S.L., Semmler, W., 2011. Cilengitide inhibits progression of experimental breast cancer bone metastases as imaged noninvasively using VCT, MRI and DCE-MRI in a longitudinal in vivo study. International Journal of Cancer 128, 2453–2462. https://doi.org/https://doi.org/10.1002/ijc.25563

Berthold, F., Faldum, A., Ernst, A., Boos, J., Dilloo, D., Eggert, A., Fischer, M., Frühwald, M., Henze, G., Klingebiel, T., Kratz, C., Kremens, B., Krug, B., Leuschner, I., Schmidt, M., Schmidt, R., Schumacher-Kuckelkorn, R., von Schweinitz, D., Schilling, F.H., Theissen, J., Volland, R., Hero, B., Simon, T., 2020. Extended induction chemotherapy does not improve the outcome for high-risk neuroblastoma patients: results of the randomized open-label GPOH trial NB2004-HR. Annals of Oncology 31, 422–429. https://doi.org/https://doi.org/10.1016/j.annonc.2019.11.011

Brodeur, G.M., Sekhon, G.S., Goldstein, M.N., 1977. Chromosomal aberrations in human neuroblastomas. Cancer 40, 2256–2263. https://doi.org/https://doi.org/10.1002/1097-0142(197711)40:5<2256::AID-CNCR2820400536>3.0.CO;2-1

Burgos-Panadero, R., Noguera, I., Cañete, A., Navarro, S., Noguera, R., 2019. Vitronectin as a molecular player of the tumor microenvironment in neuroblastoma. BMC Cancer 19, 479. https://doi.org/10.1186/s12885-019-5693-2

Cacho-Díaz, B., García-Botello, D.R., Wegman-Ostrosky, T., Reyes-Soto, G., Ortiz-Sánchez, E., Herrera-Montalvo, L.A., 2020. Tumor microenvironment differences between primary tumor and brain metastases. Journal of Translational Medicine 18, 1. https://doi.org/10.1186/s12967-019-02189-8

Carpenter, E.L., Rader, J., Ruden, J., Rappaport, E.F., Hunter, K.N., Hallberg, P.L., Krytska, K., O'Dwyer, P.J., Mosse, Y.P., 2014. Dielectrophoretic Capture and Genetic Analysis of Single Neuroblastoma Tumor Cells . Frontiers in Oncology .

Chandrasekar, N., Mohanam, S., Gujrati, M., Olivero, W.C., Dinh, D.H., Rao, J.S., 2003. Downregulation of uPA inhibits migration and PI3k/Akt signaling in glioblastoma cells. Oncogene 22, 392–400. https://doi.org/10.1038/sj.onc.1206164

Chen, M.-L., Lai, C.-J., Lin, Y.-N., Huang, C.-M., Lin, Y.-H., 2020. Multifunctional nanoparticles for targeting the tumor microenvironment to improve synergistic drug combinations and cancer treatment effects. Journal of Materials Chemistry B 8, 10416–10427. https://doi.org/10.1039/D0TB01733G

Cheng, N.C., van Zandwijk, N., Reid, G., 2014. Cilengitide inhibits attachment and invasion of malignant pleural mesothelioma cells through antagonism of integrins αvβ3 and αvβ5. PloS one 9, e90374–e90374. https://doi.org/10.1371/journal.pone.0090374

Chou, T.C., 2010. Drug combination studies and their synergy quantification using the chou-talalay method. Cancer Research 70, 440–446. https://doi.org/10.1158/0008-5472.CAN-09-1947

Cox, T.R., 2021. The matrix in cancer. Nature Reviews Cancer 21, 217–238. https://doi.org/10.1038/s41568-020-00329-7

Craig, A.J., von Felden, J., Garcia-Lezana, T., Sarcognato, S., Villanueva, A., 2020. Tumour evolution in hepatocellular carcinoma. Nature Reviews Gastroenterology & Hepatology 17, 139–152. https://doi.org/10.1038/s41575-019-0229-4

Desgrosellier, J.S., Cheresh, D.A., 2010. Integrins in cancer: biological implications and therapeutic opportunities. Nature Reviews Cancer 10, 9–22. https://doi.org/10.1038/nrc2748

DeVita VT, Lawrence TS, R.S., 2008. Solid tumours of childhood, in: Cancer: Principles and Practice of Oncology. pp. 2043–84.

El Moukhtari, S.H., Rodríguez-Nogales, C., Blanco-Prieto, M.J., 2021. Oral lipid nanomedicines: current status and future perspectives in cancer treatment. Advanced drug delivery reviews. https://doi.org/10.1016/j.addr.2021.03.004

Erdreich-Epstein, A., Shimada, H., Groshen, S., Liu, M., Metelitsa, L.S., Kim, K.S., Stins, M.F., Seeger, R.C., Durden, D.L., 2000. Integrins α(v)β3 and α(v)β5 are expressed by endothelium of high- risk neuroblastoma and their inhibition is associated with increased endogenous ceramide. Cancer Research 60, 712–721.

Erdreich-Epstein, A., Singh, A.R., Joshi, S., Vega, F.M., Guo, P., Xu, J., Groshen, S., Ye, W., Millard, M., Campan, M., Morales, G., Garlich, J.R., Laird, P.W., Seeger, R.C., Shimada, H., Durden, D.L., 2016. Association of high microvessel α v β 3 and low PTEN with poor outcome in stage 3 neuroblastoma: rationale for using first in class dual PI3K/BRD4 inhibitor, SF1126. Oncotarget; Vol 8, No 32.

Estella-Hermoso de Mendoza, A., Rayo, M., Mollinedo, F., Blanco-Prieto, M.J., 2008. Lipid nanoparticles for alkyl lysophospholipid edelfosine encapsulation: Development and in vitro characterization. European Journal of Pharmaceutics and Biopharmaceutics 68, 207–213. https://doi.org/10.1016/j.ejpb.2007.06.015

Fares, J., Fares, M.Y., Khachfe, H.H., Salhab, H.A., Fares, Y., 2020. Molecular principles of metastasis: a hallmark of cancer revisited. Signal Transduction and Targeted Therapy 5, 28. https://doi.org/10.1038/s41392-020-0134-x

Garbayo, E., Pascual-Gil, S., Rodríguez-Nogales, C., Saludas, L., Estella-Hermoso de Mendoza, A., Blanco-Prieto, M.J., 2020. Nanomedicine and drug delivery systems in cancer and regenerative medicine. Wiley Interdisciplinary Reviews: Nanomedicine and Nanobiotechnology 1–22. https://doi.org/10.1002/wnan.1637

Gilbert, M.R., Kuhn, J., Lamborn, K.R., Lieberman, F., Wen, P.Y., Mehta, M., Cloughesy, T., Lassman, A.B., DeAngelis, L.M., Chang, S., Prados, M., 2012. Cilengitide in patients with recurrent glioblastoma: the results of NABTC 03-02, a phase II trial with measures of treatment delivery. Journal of Neuro-Oncology 106, 147–153. https://doi.org/10.1007/s11060-011-0650-1

González-Fernández, Y., Brown, H.K., Patiño-García, A., Heymann, D., Blanco-Prieto, M.J., 2018. Oral administration of edelfosine encapsulated lipid nanoparticles causes regression of lung metastases in pre-clinical models of osteosarcoma. Cancer Letters. https://doi.org/10.1016/j.canlet.2018.05.030

González-Fernández, Y., Imbuluzqueta, E., Zalacain, M., Mollinedo, F., Patiño-García, A., Blanco-Prieto, M.J., 2017. Doxorubicin and edelfosine lipid nanoparticles are effective acting synergistically against drug-resistant osteosarcoma cancer cells. Cancer Letters 388, 262–268. https://doi.org/10.1016/j.canlet.2016.12.012

Haddad, T., Qin, R., Lupu, R., Satele, D., Eadens, M., Goetz, M.P., Erlichman, C., Molina, J., 2017. A phase I study of cilengitide and paclitaxel in patients with advanced solid tumors. Cancer Chemotherapy and Pharmacology 79, 1221–1227. https://doi.org/10.1007/s00280-017-3322-9

Handorf, A.M., Zhou, Y., Halanski, M.A., Li, W.-J., 2015. Tissue Stiffness Dictates Development, Homeostasis, and Disease Progression. Organogenesis 11, 1–15. https://doi.org/10.1080/15476278.2015.1019687

Harenza, J.L., Diamond, M.A., Adams, R.N., Song, M.M., Davidson, H.L., Hart, L.S., Dent, M.H., Fortina, P., Reynolds, C.P., Maris, J.M., 2017. Transcriptomic profiling of 39 commonly-used neuroblastoma cell lines. Scientific Data 4, 170033. https://doi.org/10.1038/sdata.2017.33

Harjunpää, H., Llort Asens, M., Guenther, C., Fagerholm, S.C., 2019. Cell Adhesion Molecules and Their Roles and Regulation in the Immune and Tumor Microenvironment . Frontiers in Immunology .

Hu, C.-M.J., Zhang, L., 2012. Nanoparticle-based combination therapy toward overcoming drug resistance in cancer. Biochemical Pharmacology 83, 1104–1111. https://doi.org/10.1016/j.bcp.2012.01.008

Joshi, M.D., Müller, R.H., 2009. Lipid nanoparticles for parenteral delivery of actives. European Journal of Pharmaceutics and Biopharmaceutics. https://doi.org/10.1016/j.ejpb.2008.09.003

Kalli, M., Stylianopoulos, T., 2018. Defining the Role of Solid Stress and Matrix Stiffness in Cancer Cell Proliferation and Metastasis . Frontiers in Oncology .

Keck, C.M., Müller, R.H., 2013. Nanotoxicological classification system (NCS) - A guide for the risk-benefit assessment of nanoparticulate drug delivery systems. European Journal of Pharmaceutics and Biopharmaceutics 84, 445–448. https://doi.org/10.1016/j.ejpb.2013.01.001

Kenny, H.A., Kaur, S., Coussens, L.M., Lengyel, E., 2008. The initial steps of ovarian cancer cell metastasis are mediated by MMP-2 cleavage of vitronectin and fibronectin. The Journal of Clinical Investigation 118, 1367–1379. https://doi.org/10.1172/JCI33775

Keshelava, N., Seeger, R.C., Groshen, S., Reynolds, C.P., 1998. Drug resistance patterns of human neuroblastoma cell lines derived from patients at different phases of therapy. Cancer Research 58, 5396–5405.

Kryh, H., Carén, H., Erichsen, J., Sjöberg, R.-M., Abrahamsson, J., Kogner, P., Martinsson, T., 2011. Comprehensive SNP array study of frequently used neuroblastoma cell lines; copy neutral loss of heterozygosity is common in the cell lines but uncommon in primary tumors. BMC Genomics 12, 443. https://doi.org/10.1186/1471-2164-12-443

Lange, B., Schroeder, U., Huebener, N., Jikai, J., Wenkel, J., Strandsby, A., Wrasidlo, W., Gaedicke, G., Lode, H.N., 2003. Rationally designed hydrolytically activated etoposide prodrugs, a novel strategy for the treatment of neuroblastoma. Cancer Letters 197, 225–230. https://doi.org/10.1016/S0304-3835(03)00106-X

Lasa-Saracíbar, B., Aznar, M.Á., Lana, H., Aizpún, I., Gil, A.G., Blanco-Prieto, M.J., 2014. Lipid nanoparticles protect from edelfosine toxicity in vivo. International Journal of Pharmaceutics 474, 1–5. https://doi.org/10.1016/j.ijpharm.2014.07.053

Lasa-Saracibar, B., Estella-Hermoso de Mendoza, A., Guada, M., Dios-Vieitez, C., Blanco-Prieto, M.J., 2012. Lipid nanoparticles for cancer therapy: state of the art and future prospects. Expert Opinion on Drug Delivery 9, 1245–1261. https://doi.org/10.1517/17425247.2012.717928

Leblond, P., Dewitte, A., Le Tinier, F., Bal-Mahieu, C., Baroncini, M., Sarrazin, T., Lartigau, E., Lansiaux, A., Meignan, S., 2013. Cilengitide targets pediatric glioma and neuroblastoma cells through cell detachment and anoikis induction. Anti-Cancer Drugs 24, 818–825. https://doi.org/10.1097/CAD.0b013e328362edc5

Lee, S.L., Cabanero, M., Hyrcza, M., Butler, M., Liu, F.-F., Hansen, A., Huang, S.H., Tsao, M.-S., Song, Y., Lu, L., Xu, W., Chepeha, D.B., Goldstein, D.P., Weinreb, I., Bratman, S. V, 2019. Computer-assisted image analysis of the tumor microenvironment on an oral tongue squamous cell carcinoma tissue microarray. Clinical and Translational Radiation Oncology 17, 32–39. https://doi.org/https://doi.org/10.1016/j.ctro.2019.05.001

Let's talk about lipid nanoparticles, 2021. . Nature Reviews Materials 6, 99–99. https://doi.org/10.1038/s41578-021-00281-4

Li, P., Gao, Y., Ji, Z., Zhang, X., Xu, Q., Li, G., Guo, Z., Zheng, B., Guo, X., 2004. Role of urokinase plasminogen activator and its receptor in metastasis and invasion of neuroblastoma. Journal of Pediatric Surgery 39, 1512–1519. https://doi.org/https://doi.org/10.1016/j.jpedsurg.2004.06.011

Liang, C., Xu, L., Song, G., Liu, Z., 2016. Emerging nanomedicine approaches fighting tumor metastasis: animal models, metastasis-targeted drug delivery, phototherapy, and immunotherapy. Chemical Society Reviews 45, 6250–6269. https://doi.org/10.1039/C6CS00458J

López-Carrasco, A., Martín-Vañó, S., Burgos-Panadero, R., Monferrer, E., Berbegall, A.P., Fernández-Blanco, B., Navarro, S., Noguera, R., 2020. Impact of extracellular matrix stiffness on genomic heterogeneity in MYCN-amplified neuroblastoma cell line. Journal of Experimental & Clinical Cancer Research 39, 226. https://doi.org/10.1186/s13046-020-01729-1

Lu, P., Weaver, V.M., Werb, Z., 2012. The extracellular matrix: A dynamic niche in cancer progression. Journal of Cell Biology 196, 395–406. https://doi.org/10.1083/jcb.201102147

Mas-Moruno, C., Rechenmacher, F., Kessler, H., 2010. Cilengitide: The First Anti-Angiogenic Small Molecule Drug Candidate. Design, Synthesis and Clinical Evaluation. Anti-Cancer Agents in Medicinal Chemistry 10, 753–768. https://doi.org/10.2174/187152010794728639

Matthay, K.K., Maris, J.M., Schleiermacher, G., Nakagawara, A., Mackall, C.L., Diller, L., Weiss, W.A., 2016. Neuroblastoma. Nature Reviews Disease Primers 2. https://doi.org/10.1038/nrdp.2016.78

Moreno-Layseca, P., Streuli, C.H., 2014. Signalling pathways linking integrins with cell cycle progression. Matrix Biology 34, 144–153. https://doi.org/https://doi.org/10.1016/j.matbio.2013.10.011

Ortega-Martínez, I., Gardeazabal, J., Erramuzpe, A., Sanchez-Diez, A., Cortés, J., García-Vázquez, M.D., Pérez-Yarza, G., Izu, R., Luís Díaz-Ramón, J., de la Fuente, I.M.,

Asumendi, A., Boyano, M.D., 2016. Vitronectin and dermcidin serum levels predict the metastatic progression of AJCC I–II early-stage melanoma. International Journal of Cancer 139, 1598–1607. https://doi.org/https://doi.org/10.1002/ijc.30202

Overchuk, M., Zheng, G., 2018. Overcoming obstacles in the tumor microenvironment: Recent advancements in nanoparticle delivery for cancer theranostics. Biomaterials 156, 217–237. https://doi.org/https://doi.org/10.1016/j.biomaterials.2017.10.024

Relling, M. V., Yanishevski, Y., Nemec, J., Evans, W.E., Boyett, J.M., Behm, F.C., Pui, C.H., 1998. Etoposide and antimetabolite pharmacology in patients who develop secondary acute myeloid leukemia. Leukemia 12, 346–352. https://doi.org/10.1038/sj.leu.2400928

Ren, B., Cui, M., Yang, G., Wang, H., Feng, M., You, L., Zhao, Y., 2018. Tumor microenvironment participates in metastasis of pancreatic cancer. Molecular Cancer 17, 108. https://doi.org/10.1186/s12943-018-0858-1

Ribeiro Franco, P.I., Rodrigues, A.P., de Menezes, L.B., Pacheco Miguel, M., 2020. Tumor microenvironment components: Allies of cancer progression. Pathology - Research and Practice 216, 152729. https://doi.org/https://doi.org/10.1016/j.prp.2019.152729

Schneider, G., Suszynska, M., Kakar, S., Ratajczak, M.Z., 2016. Vitronectin in the ascites of human ovarian carcinoma acts as a potent chemoattractant for ovarian carcinoma: Implication for metastasis by cancer stem cells. Journal of cancer stem cell research 4, e1005. https://doi.org/10.14343/JCSCR.2016.4e1005

Shi, K., Lan, R.-L., Tao, X., Wu, C.-Y., Hong, H.-F., Lin, J.-H., 2015. Vitronectin significantly influences prognosis in osteosarcoma. International journal of clinical and experimental pathology 8, 11364–11371.

Stock, C., Bozsaky, E., Watzinger, F., Poetschger, U., Orel, L., Lion, T., Kowalska, A., Ambros, P.F., 2008. Genes Proximal and Distal to MYCN Are Highly Expressed in Human Neuroblastoma as Visualized by Comparative Expressed Sequence Hybridization. The American Journal of Pathology 172, 203–214. https://doi.org/https://doi.org/10.2353/ajpath.2008.061263

Stupp, R., Hegi, M.E., Gorlia, T., Erridge, S.C., Perry, J., Hong, Y.K., Aldape, K.D., Lhermitte, B., Pietsch, T., Grujicic, D., Steinbach, J.P. eter, Wick, W., Tarnawski, R., Nam, D.H., Hau, P., Weyerbrock, A., Taphoorn, M.J.B., Shen, C.C., Rao, N., Thurzo, L., Herrlinger, U., Gupta, T., Kortmann, R.D., Adamska, K., McBain, C., Brandes, A.A., Tonn, J.C. hristian, Schnell, O., Wiegel, T., Kim, C.Y., Nabors, L.B. urt, Reardon, D.A., van den Bent, M.J., Hicking, C., Markivskyy, A., Picard, M., Weller, M., 2014a. Cilengitide combined with standard treatment for patients with newly diagnosed glioblastoma with methylated MGMT promoter (CENTRIC EORTC 26071-22072 study): a multicentre, randomised, open-label, phase 3 trial. The Lancet. Oncology 15, 1100–1108. https://doi.org/10.1016/S1470-2045(14)70379-1

Stupp, R., Picard, M., Weller, M., 2014b. Does cilengitide deserve another chance? The Lancet Oncology 15, e585–e586. https://doi.org/10.1016/S1470-2045(14)71121-0

Sugiura, Y., Ma, L., Sun, B., Shimada, H., Laug, W.E., Seeger, R.C., DeClerck, Y.A., 1999. The Plasminogen-Plasminogen Activator (PA) System in Neuroblastoma. Cancer Research 59, 1327 LP – 1336.

Tabatabai, G., 2017. The Role of Integrins in Angiogenesis BT - Biochemical Basis and Therapeutic Implications of Angiogenesis, in: Mehta, J.L., Mathur, P., Dhalla, N.S. (Eds.), . Springer International Publishing, Cham, pp. 23–36. https://doi.org/10.1007/978-3-319-61115-0_2

Tadeo, I., Berbegall, A.P., Castel, V., García-Miguel, P., Callaghan, R., Påhlman, S., Navarro, S., Noguera, R., 2016. Extracellular matrix composition defines an ultra-high-risk group of neuroblastoma within the high-risk patient cohort. British Journal of Cancer 115, 480–489. https://doi.org/10.1038/bjc.2016.210

Tadeo, I., Berbegall, A.P., Navarro, S., Castel, V., Noguera, R., 2017. A stiff extracellular matrix is associated with malignancy in peripheral neuroblastic tumors. Pediatric Blood & Cancer 64, e26449. https://doi.org/https://doi.org/10.1002/pbc.26449

Tadeo, I., Bueno, G., Berbegall, A.P., Milagro Fernández-Carrobles, M., Castel, V., García-Rojo, M., Navarro, S., Noguera, R., n.d. Vascular patterns provide therapeutic targets in aggressive neuroblastic tumors.

Tsai, M.-J., Chang, W.-A., Huang, M.-S., Kuo, P.-L., 2014. Tumor microenvironment: a new treatment target for cancer. ISRN biochemistry 2014, 351959. https://doi.org/10.1155/2014/351959

van Wezel, E.M., van Zogchel, L.M.J., van Wijk, J., Timmerman, I., Vo, N.-K., Zappeij-Kannegieter, L., deCarolis, B., Simon, T., van Noesel, M.M., Molenaar, J.J., van Groningen, T., Versteeg, R., Caron, H.N., van der Schoot, C.E., Koster, J., van Nes, J., Tytgat, G.A.M., 2019. Mesenchymal Neuroblastoma Cells Are Undetected by Current mRNA Marker Panels: The Development of a Specific Neuroblastoma Mesenchymal Minimal Residual Disease Panel. JCO Precision Oncology 1–11. https://doi.org/10.1200/PO.18.00413

Vansteenkiste, J., Barlesi, F., Waller, C.F., Bennouna, J., Gridelli, C., Goekkurt, E., Verhoeven, D., Szczesna, A., Feurer, M., Milanowski, J., Germonpre, P., Lena, H., Atanackovic, D., Krzakowski, M., Hicking, C., Straub, J., Picard, M., Schuette, W., O'Byrne, K., 2015. Cilengitide combined with cetuximab and platinum-based chemotherapy as first-line treatment in advanced non-small-cell lung cancer (NSCLC) patients: results of an open-label, randomized, controlled phase II study (CERTO). Annals of Oncology 26, 1734–1740. https://doi.org/https://doi.org/10.1093/annonc/mdv219

Vicente-Munuera, P., Burgos-Panadero, R., Noguera, I., Navarro, S., Noguera, R., Escudero, L.M., 2020. The topology of vitronectin: A complementary feature for neuroblastoma risk classification based on computer-aided detection. International Journal of Cancer 146, 553–565. https://doi.org/https://doi.org/10.1002/ijc.32495

Xu, J., Mosher, D., 2011. Fibronectin and Other Adhesive Glycoproteins, in: Mecham, R.P. (Ed.), The Extracellular Matrix: An Overview. Springer Berlin Heidelberg, Berlin, Heidelberg, pp. 41–75. https://doi.org/10.1007/978-3-642-16555-9_2

Yang, F., Zhao, Z., Sun, B., Chen, Q., Sun, J., He, Z., Luo, C., 2020. Nanotherapeutics for Antimetastatic Treatment. Trends in Cancer 6, 645–659. https://doi.org/https://doi.org/10.1016/j.trecan.2020.05.001

Zhao, C.-Y., Cheng, R., Yang, Z., Tian, Z.-M., 2018. Nanotechnology for Cancer Therapy Based on Chemotherapy. Molecules . https://doi.org/10.3390/molecules23040826

Zhu, W., Li, W., Yang, G., Fu, C., Jiang, G., Hu, Q., 2014. Vitronectin silencing inhibits hepatocellular carcinoma in vitro and in vivo. Future Oncology 11, 251–258. https://doi.org/10.2217/fon.14.202

Zormpas-Petridis, K., Noguera, R., Ivankovic, D.K., Roxanis, I., Jamin, Y., Yuan, Y., 2021. SuperHistopath: A Deep Learning Pipeline for Mapping Tumor Heterogeneity on Low-Resolution Whole-Slide Digital Histopathology Images . Frontiers in Oncology .

CrediT autor statement

Author Contributions: R.B-P. wrote the first draft preparation of human, *in vitro* and *in vivo* studies; S.H.E. wrote the first draft regarding the development of nanomedicines and *in vitro* efficacy and combination studies; R.B.-P. and I.N. performed the experiments on mice; S.H.E. and C.R.N. were involved in the development of nanomedicines, *in vitr*o efficacy experiments and drug combination study; S.M-V. performed human and mice genetic analysis; R.B-P. and

P.V-M designed the digital analysis; A.C. provided clinic data; R.B.-P. and S.N. performed immunohistochemical analysis and microscopic assessment of human, *in vitro* and *in vivo* samples; MJ.B-P. conceived, designed and supervised the development of nanomedicines, *in vitr*o efficacy and drug combination study ; R. N. conceived, design and supervised human, *in vitro* and *in vivo* studies. All authors read and agreed to the published version of the manuscript.

June 1st, 2021

Conflict of Interest Disclosure Statement

We wish to confirm that there are no known conflicts of interest associated with this publication and there has been no significant financial support for this work that could have influenced its outcome.

We confirm that the manuscript has been read and approved by all named authors and that there are no other persons who satisfied the criteria for authorship but are not listed. We further confirm that the order of authors listed in the manuscript has been approved by all of us.

We confirm that we have given due consideration to the protection of intellectual property associated with this work and that there are no impediments to publication, including the timing of publication, with respect to intellectual property. In so doing we confirm that we have followed the regulations of our institutions concerning intellectual property.

We further confirm that any aspect of the work covered in this manuscript that has involved either experimental animals or human patients has been conducted with the ethical approval of all relevant bodies and that such approvals are acknowledged within the manuscript.

We understand that the Corresponding Author is the sole contact for the Editorial process (including Editorial Manager and direct communications with the office). He/she is responsible for communicating with the other authors about progress, submissions of revisions and final approval of proofs. We confirm that we have provided a current, correct email address which is accessible by the Corresponding Author and which has been configured to accept email from María Blanco-Prieto, mjblanco@unav.es